Molecular Crystals and Liquid Crystals Science and Technology. Section A. Molecular Crystals and Liquid Crystals

Publication details, including instructions for authors and subscription information:
http://www.tandfonline.com/loi/gmcl19

3D Imaging and Simulation of the Polarisation Distribution in Molecular Crystals

Andrea Quintel [a], Stephan W. Roth [a], Jürg Hulliger [a] & Michael Wübbenhorst [b]

[a] Department of Chemistry and Biochemistry, University of Berne, Freiestrasse 3, 3012, Berne, Switzerland

[b] Department of Polymer Technology, Delft University of Technology, P. O. Box 5045, 2600, GA Delft, The Netherlands

Version of record first published: 27 Oct 2006

To cite this article: Andrea Quintel, Stephan W. Roth, Jürg Hulliger & Michael Wübbenhorst (2000): 3D Imaging and Simulation of the Polarisation Distribution in Molecular Crystals, Molecular Crystals and Liquid Crystals Science and Technology. Section A. Molecular Crystals and Liquid Crystals, 338:1, 243-256

To link to this article: http://dx.doi.org/10.1080/10587250008024433

Mol. Cryst. Liq. Cryst., Vol. 338, pp. 243-256
Reprints available directly from the publisher
Photocopying permitted by license only

3D Imaging and Simulation of the Polarisation Distribution in Molecular Crystals

ANDREA QUINTEL[a], STEPHAN W. ROTH[a], JÜRG HULLIGER[a*] and MICHAEL WÜBBENHORST[b†]

[a]Department of Chemistry and Biochemistry, University of Berne, Freiestrasse 3, 3012 Berne, Switzerland and [b]Department of Polymer Technology, Delft University of Technology, P.O. Box 5045, 2600 GA Delft, The Netherlands

(Received January 06, 1999; In final form May 13, 1999)

The spatial polarisation distribution in inhomogeneously polar molecular crystals has been imaged by scanning pyroelectric tomography and simulated by a Markov process. The experimental technique combines scanning pyroelectric microscopy (SPEM) with layerwise thinning of crystals. The SPEM probes the local spontaneous polarisation by its temperature dependence (pyroelectric effect). A focused and intensity modulated laser beam scans the surface of a polar sample and induces temperature changes in a volume depending on the laser spot size and the thermal diffusion length λ_{th}. Since high lateral resolution of the SPEM is only available for small values of λ_{th}, depth information to a resolution of ~10 μm is achieved by repeated scanning and stepwise thinning of crystals. A layer by layer technique can provide 3D imaging of the polar ordering with a lateral resolution of ~ 20 μm at a probed layer thickness of ~ 10 μm. Applied to perhydrotriphenylene (PHTP) co-crystallised with 1-(4-nitrophenyl)piperazine (NPP) two conical macro-domains of opposite and nearly constant polarisation were found. The SPEM results are in good agreement with a homogeneous Markov chain model driving dipolar molecules into a parallel state within channels of PHTP. The new tomographic view reveals that the opposing cones are partially overlapping at the tips. Lateral growth processes are assumed to be responsible for this. A theoretical section covers aspects of the convergency into the polar state and the length of polar chains discussed in terms of intermolecular interaction energies.

Keywords: pyroelectricity; scanning probe microscopy; tomography; inclusion compound; Markov process

* Fax. +41 31 631 39 93, Email: juerg.hulliger@iac.unibe.ch
† Email: wuebbenhorst@stm.tudelft.nl

1. INTRODUCTION

The acentric packing of dipolar molecules is one way to establish a permanent electrical polarisation in molecular crystals. Most of these pyroelectric and/or piezoelectric organic single crystals show in principle a spatially *homogeneous* polarisation. However, intrinsic (orientational disorder[1]) or extrinsic (impurities[2]) defects can give rise to an *inhomogeneous* distribution of the electrical polarisation.

There are two recently developed scanning probe techniques potentially available to image the local polarisation: near-field optical second-harmonic microscopy (SHG-SNOM)[3] and electrostatic force microscopy[4]. Although their lateral resolution limits might be below 10–100 nm, applications are restricted to a certain surface smoothness in order to avoid a dependence of the SHG or electrostatic signal mainly on topography. SHG-SNOM and SHG-microscopy in the far-field mode of operation[5] are furthermore restricted to acentric molecular materials which molecular building bricks are sufficiently hyperpolarisable.

Scanning *pyroelectric microscopy* (SPEM) permits the probing of the permanent polarisation with a sensitivity which depends on (i) the resolution of the optical excitation path, (ii) the thermal diffusion length and (iii) the pyroelectric coefficient of the material. Since SPEM is based on the pyroelectric effect, many acentric arrangements of molecules with permanent dipole moments are potentially accessible by this technique. Recently, we have demonstrated the capability of SPEM for the determination of the surface polarisation distribution in molecular crystals[6,7]. In the present paper we extend the SPEM to a *tomographic technique* for the imaging of the 3D polarisation distribution. The material we consider here is a perhydrotriphenylene (PHTP) inclusion compound with 1-(4-nitrophenyl)piperazine (NPP) as one of the many possible guest molecules[8]. In the supramolecular assembly, PHTP molecules form stacks which enclose parallel chains of dipolar molecules[8].

Several basic issues are addressed in the following sections: (I) Revealing the overlapping of the cones at the tips by improvement of the SPEM technique. (II) The influence of intermolecular interaction energies on (i) the cone formation, (ii) the minimum growth length along the channel axis in order to achieve a constant value of polarity, and (iii) the mean chain length between two dipole reversals.

2. THE METHOD OF SCANNING PYROELECTRIC TOMOGRAPHY

In the thermally and mechanically unperturbed state, the intrinsic polarisation P of a polar material is normally compensated by outer charges. This charge compensation, however, can be disturbed by a rapid change in temperature resulting in net

surface charges due to the *pyroelectric* effect ($p = \frac{dP}{dT}$, p: pyroelectric coefficient). A detailed analysis of the pyroelectric properties of PHTP-NPP[6] revealed that thermal expansion, which reduces the dipole density ($p_3 < 0$; 3: direction of the channel axis), represents the main contribution to the pyroelectric effect in these crystals. During the mapping of the lateral distribution $p_3(x,y)$, the intensity modulated beam of a laser diode is scanned over a crystal surface which is coated by a thin absorption layer in order to ensure heat generation at the surface. The sinusoidally modulated heat flux creates a periodical temperature variation (amplitude T). This is described by a thermal wave which propagates perpendicular to the surface. The penetration depth is given by $\lambda_{th} = \sqrt{K/\pi f}$ (with $T_{x=\lambda_{th}}/T_{x=0} = 1/e$), provided that the lateral expansion of the heat is large compared to λ_{th} (planar thermal wave approximation). Under such conditions, the measured thickness of the probed surface layer depends only on the thermal diffusivity K and the modulation frequency f. The lateral resolution is roughly limited by the laser spot size (we will call this operation mode *surface*-SPEM).

In surface-SPEM, we used a lateral scanning increment of 20 μm in the x- and y-directions (Δx, Δy), which matched the laser spot diameter of about 20 μm. A modulation frequency f = 415 Hz induced a penetration depth λ_{th} of ~ 10 μm, assuming a thermal diffusivity of $K \cong 1.33 \cdot 710^{-7} m^2 s^{-1}$ for PHTP-NPP[9]. As a result, surface-SPEM probes the lateral distribution $p_3(x,y)$ in a surface layer of ~ 10 μm thickness (see Fig. 1).

In cases where polarisation information along the third dimension (depth $p_3(z)$) is to be gained, the thermal penetration length can be increased by lowering the modulation frequency. A drawback of this operation mode would, however, be that at a high penetration length $\lambda_{th} > \Delta x, \Delta y$, heat transport obeys a hemispherical heat flow[6], which reduces the lateral resolution. We therefore used an alternative way to achieve high resolution within the bulk. The present work combines surface-SPEM with layer-wise thinning of crystals. Although this layer by layer technique is destructive, it nevertheless enables 3D characterisation of the polar ordering with a lateral resolution of ~ 20 μm at a probed layer thickness of ~ 10 μm.

Crystal preparation

Growth of nearly hexagonally shaped needles of PHTP-NPP resulted from 2-butanone solutions[8]. Here, it is important to note that only crystals which grew as single crystals were used, i.e. those unperturbed from the effects of neighbouring individuals or the container wall. Crystals were thinned by means of fine abrasive paper and washed with ethanol. The crystals were covered with a light absorbing coating by dipping them in a solution of a black permanent marker dye in ethanol.

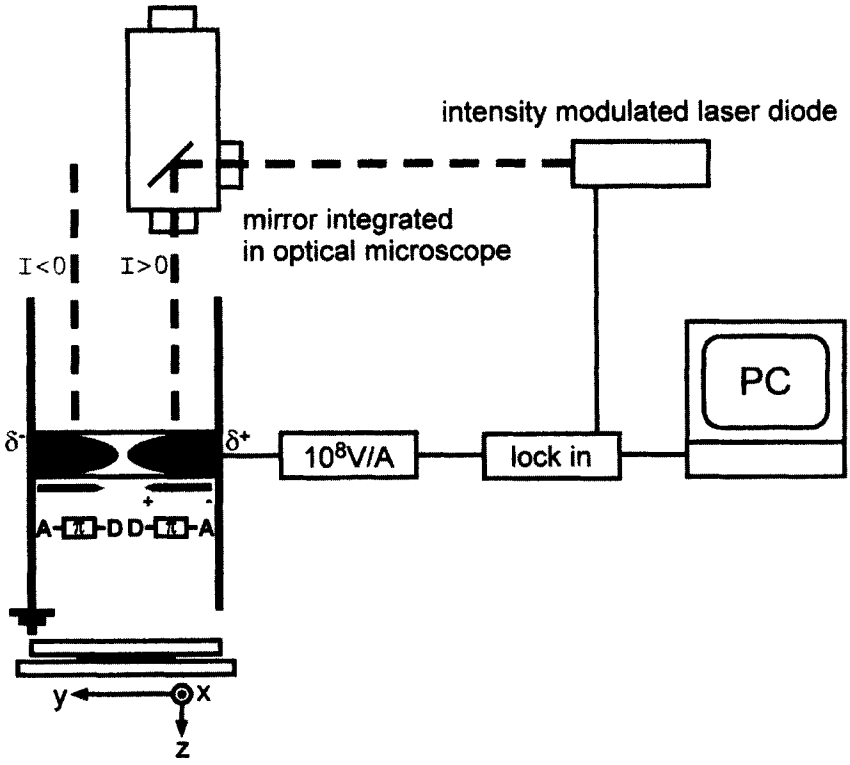

FIGURE 1 Experimental set-up. As indicated, the sample consists of two areas of opposite polarisation. Heating samples in either domain of polarisation, opposite excess charges result on both capping faces, i.e. at electrodes. This induces a discharge current flowing through the outer circuit. Depending on the heated domain, the current direction is either positive or negative (See Color Plate XVII at the back of this issue)

3. EXPERIMENTAL RESULTS AND DISCUSSION

A series of SPEM images (Fig. 2) shows the x,y dependence of the pyroelectric response on prismatic faces thinned down in steps to reach the middle section of a needle-like crystal. *Red* squares represent a positive current, whereas *blue* squares indicate a negative signal. According to Fig. 1, the current direction is directly related to the direction of the average polarisation within the heated volume. Hence, the colour intensity is a measure of the local polarisation strength. White spots represent regions of vanishing net polarisation. Obviously, $p_3(x,y,z)$ is varying in all three directions. Fig. 2 features (i) two main areas of opposite polarisation (change in sign of the current, Fig. 1), (ii) a polarisation reversal

close to the middle of the needle, and (iii) outer zones being less polarised. In Fig. 2b and c the upper part of the red conical structure is reduced stepwise, which indicates an overlapping of both domains. In particular, Fig. 2d reveals a double-cone structure of the polarisation distribution. The central zone where polarisation vanishes corresponds to the location of the seed. From the fact that PHTP-NPP develops into two cones with vanishing polarisation inbetween, we conclude that most probably the process of nucleation creates a *non polar seed* which is then subjected to a progressive mechanism of growth developing polarity (see chapter 4).

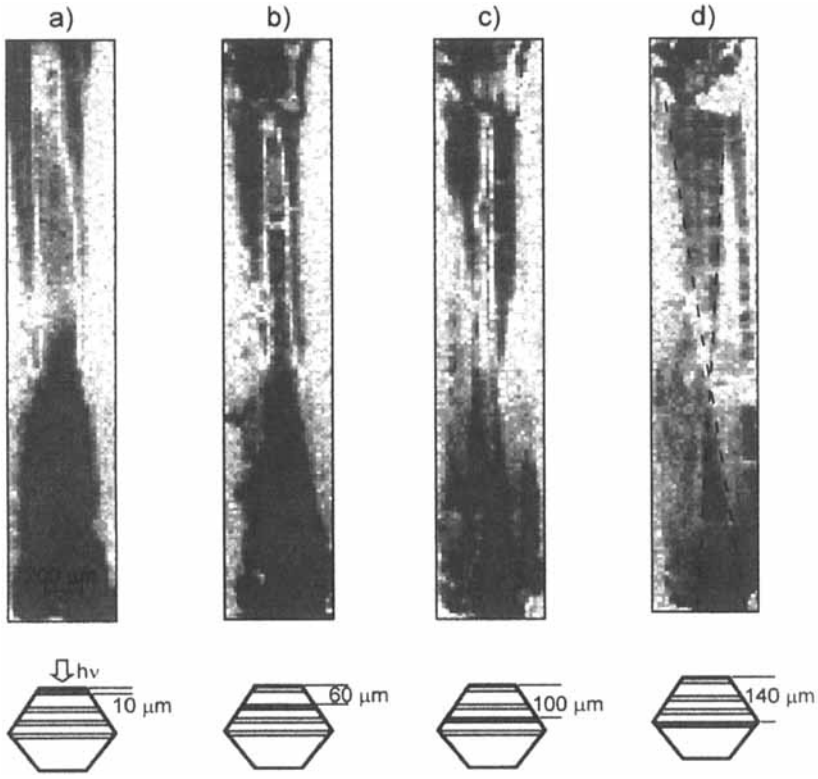

FIGURE 2 SPEM images of a PHTP-NPP single crystal thinned down in four different steps. The position dependent pyroelectric response $p_3(x,y)$ at a constant frequency f = 415 Hz is shown for four layers. Colour code: red = positive current, blue = negative current, white = zero current. Step size: 20 μm. Current range: $-0.2\ \text{pA} \leq I_{pyro} \leq 0.2\ \text{pA}$ (See Color Plate XVIII at the back of this issue)

The development of the cone, i.e. macro-domain formation, in the z-direction can be followed in Fig. 3: cross sections in the x-z plane composed from x-line

scans at constant y-positions are shown. In the tomographic view the overlapping of both cones and the development of polarisation inside the *red* domain are revealed.

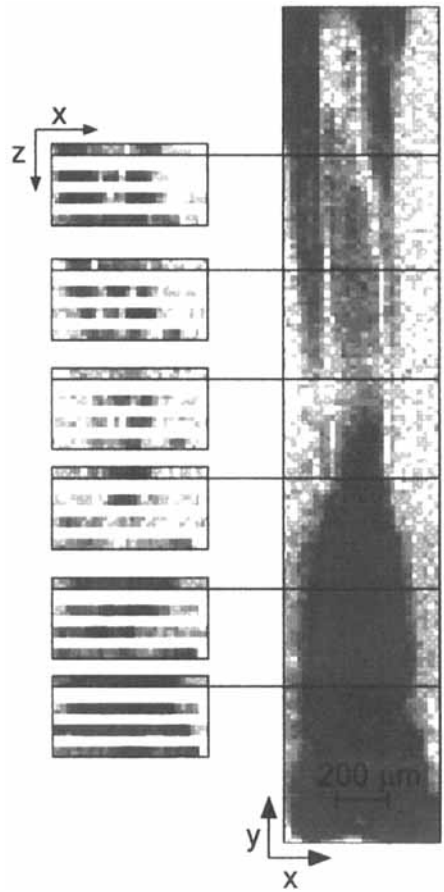

FIGURE 3 Tomographic view through the SPEM images of Fig. 2. Cross sections in the x-z plane composed from x-line scans at constant y-positions (See Color Plate XIX at the back of this issue)

4. CALCULATION AND STOCHASTIC SIMULATION OF THE POLARITY EVOLUTION

Successive growth in channel-direction (longitudinal) and perpendicular to channels (lateral) leads to a double-cone structure, which exhibits some distortion in real crystals. The deviation from the ideal geometry may be due to irregularities

in the lateral growth direction, i.e. the nucleation of new channels. There is no experimental evidence so far that the orientation of dipoles during the process of the formation of *new* channels is correlated to the polar state of the previously formed ones.

A theoretical explanation for the observed phenomena has been developed recently[10]: a Markov-type mechanism drives the orientational selective inclusion of dipolar molecules into the parallel channels of PHTP. A guest molecule can attach to the end of a chain (terminated either by ↑ or ↓) with orientation ↑ or ↓. The interaction energies between dipoles determine corresponding probabilities for ↑ or ↓ attachments. Four attachment probabilities represent the elements of a Markov matrix[10]. Set to the power of the number of attachments q, this acts as transition matrix between the *initial state* (non-polar seed) and the *polar state* after q steps. The net polarity $n_{net}(q)$ after q attachments is given by:

$$n_{net}(q) \equiv n_A(q) - n_D(q) = \frac{p_{DD} - p_{AA}}{p_{DD} + p_{AA}}(1 - \lambda^q), \qquad (1)$$

where $n_A(q)$ and $n_D(q)$ are the normalised numbers of dipole orientations ↓ or ↑, and p_{DD}, p_{AA} are the probabilities for attachments A→D···D←A, D←A···A→D (→ is indicating the direction of the dipole moment). $\lambda = 1 - p_{DD} - p_{AA}$ is one of the two eigenvalues of the Markov matrix ($\lambda' = 1$). For a definition of $n_{net}(q)$ ($0 \leq n_{net}(q) \leq 1$) we set here an equation describing a final state where $n_A(q) > n_D(q)$, which results for $E_{AA} > E_{DD}$. The corresponding equation $n_D(q) - n_A(q) = -n_{net}(q)$ holds for $n_D(q) > n_A(q)$, i. e. $E_{DD} > E_{AA}$.

The constant net polarity $n_{net}(\infty)$ for $q \to \infty$ is given by:

$$n_{net}(\infty) = \frac{P_{DD} - P_{AA}}{P_{DD} + P_{AA}} = \frac{1 - \exp(-\beta(E_{AA} - E_{DD}))}{1 + \exp(-\beta(E_{AA} - E_{DD})) + 2\exp(-\beta(E_{AA} - E_{AD}))}, \qquad (2)$$

where

$$P_{DD} = \frac{\exp(\beta(E_{AA} - E_{DD}))}{\exp(\beta(E_{AA} - E_{DD})) + \exp(\beta(E_{AA} - E_{AD}))},$$

$$P_{AA} = \frac{1}{1 + \exp(\beta(E_{AA} - E_{AD}))}, \qquad (3a, b)$$

and $\beta = 1/RT$. In cases of a large difference $E_{AA} - E_{AD}$ (strongly destabilising A···A and strongly stabilising A···D interactions) the third term in the denominator of Eq. (2) can be neglected. Therefore, $n_{net}(\infty)$ is mainly given by the difference $E_{AA} - E_{DD}$. A significant difference between E_{AA} and E_{DD} can push $n_{net}(\infty)$ to its maximum value of 1, a state where all dipoles are aligned parallel (Fig. 4).

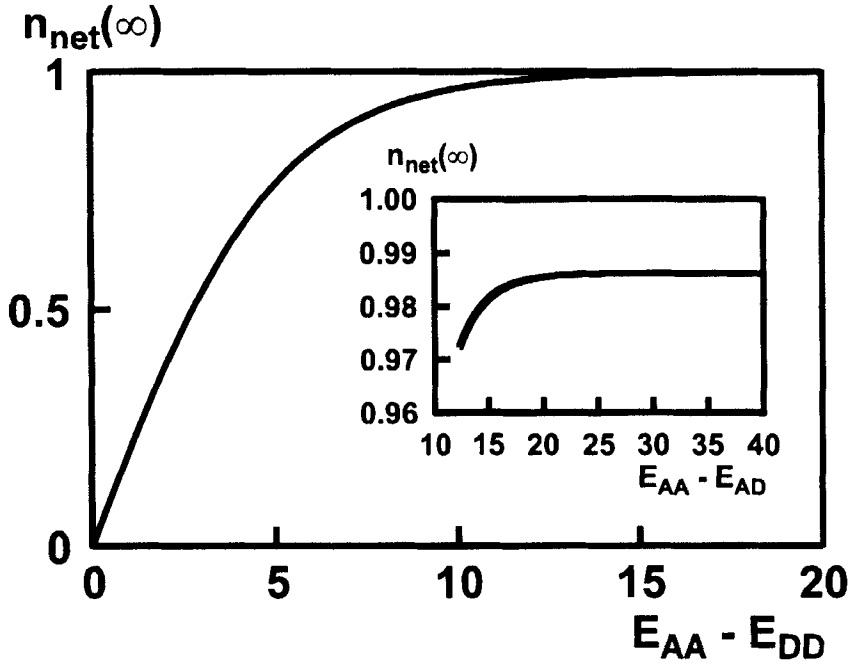

FIGURE 4 Constant net polarity $n_{net}(\infty)$ as a function of the relevant energy differences. The difference $E_{AA} - E_{DD}$ is relevant for a *high value* of net polarity, whereas the influence of $E_{AA} - E_{AD}$ on $n_{net}(\infty)$ is marginal. In both plots the third energy is fixed at the value which was calculated for NPP. All energies are in kJ mol^{-1}

For the investigated guest molecule NPP, the following values for the intermolecular interaction energies have been used[11]:

$$E_{AA} \cong 12.3 \text{ kJ mol}^{-1}, E_{DD} \cong -0.1 \text{ kJ mol}^{-1}, E_{AD} \cong -26.4 \text{ kJ mol}^{-1}.$$

These interaction energy values should be taken as a probable guess, because they were calculated for the *gas phase*, assuming the geometry as found by an X-ray analysis[12] of the inclusion compound. In reality, crystals have been obtained from solution growth, although growth from the vapour has been demonstrated. Because of $E_{AA} > E_{DD}$, we expect to find mainly A-groups at both capping faces of a growing PHTP-NPP crystal. This has already been confirmed by measurements of the *sign* of the SPEM signal[6]. Both differences are significant:

$$E_{AA} - E_{AD} \cong 38.7 \text{ kJ mol}^{-1}, \; E_{AA} - E_{DD} \cong 12.4 \text{ kJ mol}^{-1}.$$

This leads to a large value of $n_{net}(\infty) \cong 0.986$. Fig. 5 shows the behaviour of $n_{net}(q)$ in the case of NPP (solid line) and for a decreasing $E_{AA} - E_{AD}$ difference.

For NPP it takes $q \sim 10^5$ attachments to reach 90% of the stationary net polarity. In Fig. 6 both most probable lengths, $L_A = -(\ln p_{AD})^{-1}$ and $L_D = -(\ln p_{DA})^{-1}$, for sequences between two dipole reversals[12] are shown, where

$$P_{DA} = \frac{\exp(\beta(E_{AA} - E_{AD}))}{\exp(\beta(E_{AA} - E_{DD})) + \exp(\beta(E_{AA} - E_{AD}))},$$

$$P_{AD} = \frac{1}{1 + \exp(-\beta(E_{AA} - E_{AD}))}, \qquad (4a,b)$$

are the probabilities for the attachments A→D···A→D, D←A···D←A. Whereas L_A is only determined by the difference $E_{AA} - E_{AD}$, the corresponding length L_D of opposite polarity is a function of both differences (in case of $E_{AA} > E_{DD}$).

The increase of $n_{net}(q)$ is steep for q in the range of L_D. At $q << L_D$, the probability for dipole reversals becomes too low to produce significant net polarity. Production of net polarity is efficient at $q \cong L_D$ (meaning that dipole reversals are very probable) whereas at $q >> L_D$ the value of $n_{net}(\infty)$ is almost reached. Consequently, *L_D is the relevant most probable length for net polarity evolution*, because L_D is always smaller than L_A (in case of $E_{AA} > E_{DD}$, Fig. 6). This property is a function of the fundamental difference $E_{AA} - E_{DD}$, being responsible for polarity formation in the general case of condensed dipolar molecular materials[1].

In summary, *a design principle for A-π-D guest molecules* is obtained as follows: to achieve nearly $n_{net}(\infty) \cong 1$ after only a few attachment steps, the difference $|E_{AA} - E_{DD}|$ should be maximised, whereas either $|E_{AA} - E_{AD}|$ or $|E_{DD} - E_{AD}|$ should be minimised, depending on whether A- or D-groups preferably decorate the capping faces.

For a comparison between the Markov model and SPEM results we applied stochastic simulations where longitudinal and lateral growth was taken into account. Because individual channels are considered independent, such a 2D polarity development map is set up by assembling stochastic results of a certain number of channels. However, nucleation of a new channel is associated with two additional random processes: (i) the orientation of the dipole starting a new channel, and (ii) its attachment location along the length of the existing needle. All simulations started with one randomly orientated dipole in the middle of the map (Fig. 7). The *starting point* of a new polar chain (channel) was randomly generated from the total number of possible (equally probable) attachment positions (along the length of the last grown channel). This produced the *conical geometry* of the macro-domains. The orientation of the first dipole in a new channel is random. The relation between the cone length and its width is given by the ratio of channel to lateral growth velocity v_c/v_l. For a realistic ratio of growth velocities $v_c/v_l = 10/1$, an area of 10^5 layers (attachments per channel) and 10^4 channels was considered. Out of this data, squares of 10^3 layers and 10^3

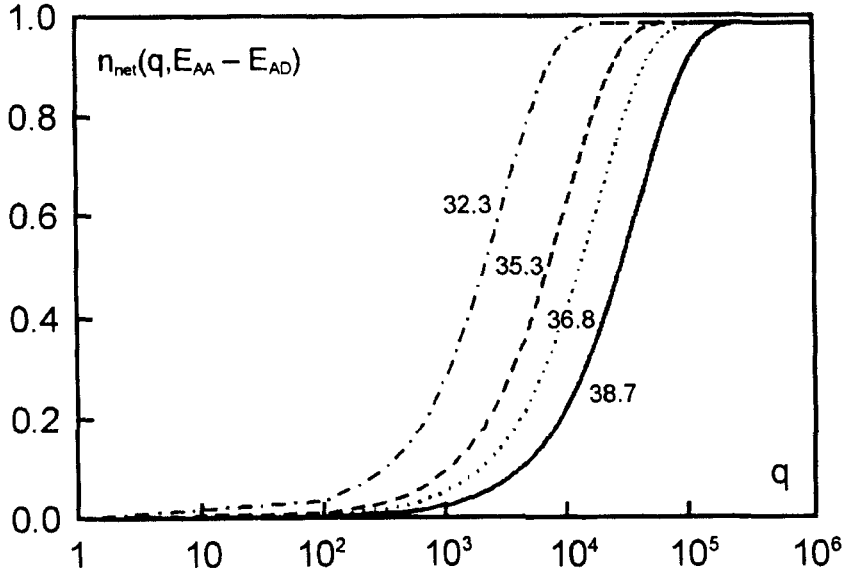

FIGURE 5 Net polarity $n_{net}(q)$ as function of the number of attachments q for NPP (solid line) and a sequence of decreasing $E_{AA} - E_{AD}$ differences (at fixed $E_{DD,\ NPP}$) used in 2D simulations (Fig. 7b-d). $q = 10^6$ corresponds to a typical length of one half of a PHTP-NPP needle crystal (~1mm). All energies are in kJ mol^{-1}

channels were summed up (corresponding to an averaging area of 1 μm^2). The resulting net polarity was normalised to one effective dipole by dividing the sum by the number of square elements (10^6). The colour intensity is therefore a measure of the *local net polarity* (red: ↑, blue: ↓, white: zero), which can be directly compared to the pyroelectric response of the *local polarisation*, as shown by SPEM images. To do this we assume an average polarisation over the probed layer thickness of ~ 10 μm. In the case of NPP, a number of 10^9 dipoles corresponds to an area of 120 × 15 μm^2 or ~ 6 SPEM spots. If we attempted to calculate the total number of spots per SPEM image (500–1000), the processing time would be above the limits of our present computing ability. Therefore, only the *polarity reversal* will be visible at the present level of *numerical* resolution (Fig. 7a). However, if we decrease the most probable lengths L_A, L_D (either by decreasing the difference $E_{AA} - E_{AD}$ (Fig. 7b-d) or increasing the difference $E_{AA} - E_{DD}$ (Fig. 7e,f)), the simulated cone's outline becomes sharper and more visible. The most probable lengths can be regarded as a kind of *scaling pattern* of cones. Present 2D polarity evolution maps correspond to SPEM images measured at a *hypothetical* lateral resolution of ~ 1 μm.

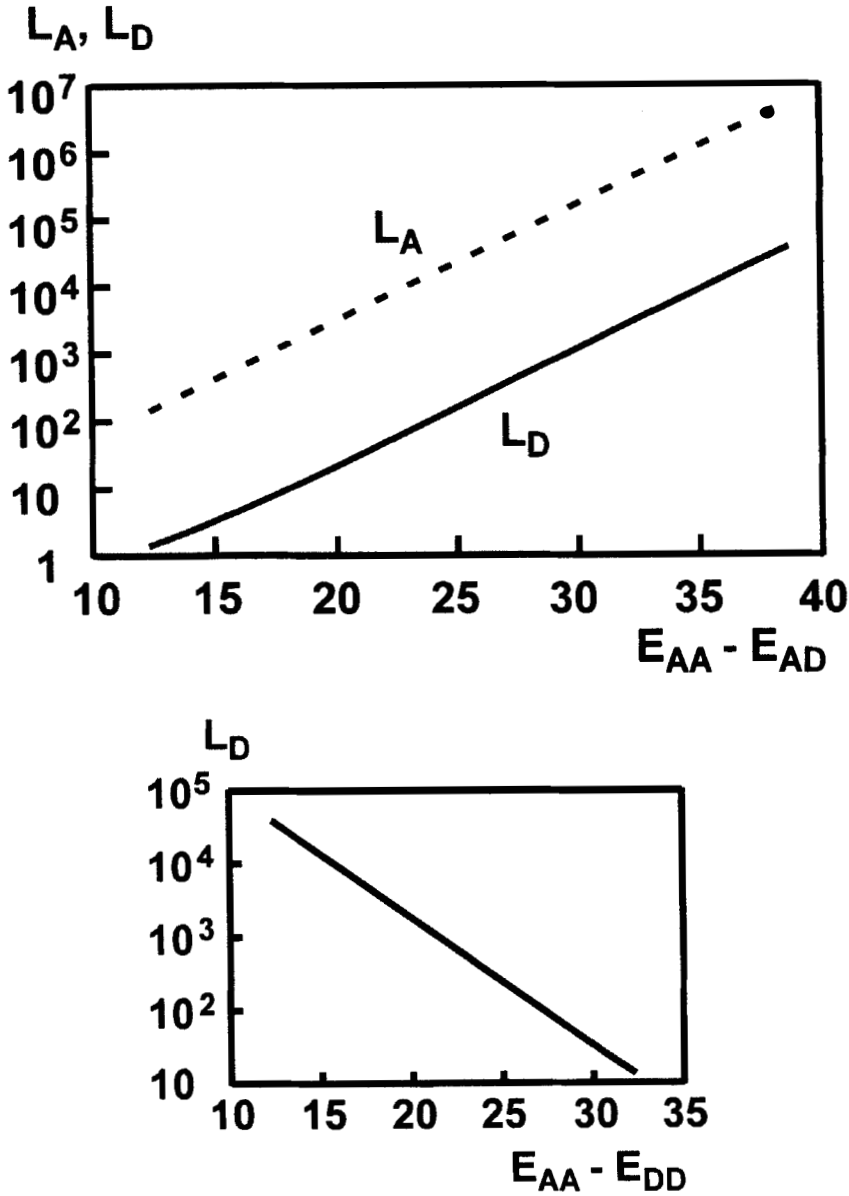

FIGURE 6 a) Most probable lengths L_A and L_D as a function of $E_{AA} - E_{AD}$ (at fixed $E_{DD, NPP}$); b) L_D as a function of $E_{AA} - E_{DD}$ (at fixed $E_{AD, NPP}$). To reduce the relevant length L_D, one may reduce the energy difference $E_{AA} - E_{AD}$ or extend $E_{AA} - E_{DD}$ by synthesising corresponding guest molecules. All energies are in kJ mol^{-1}

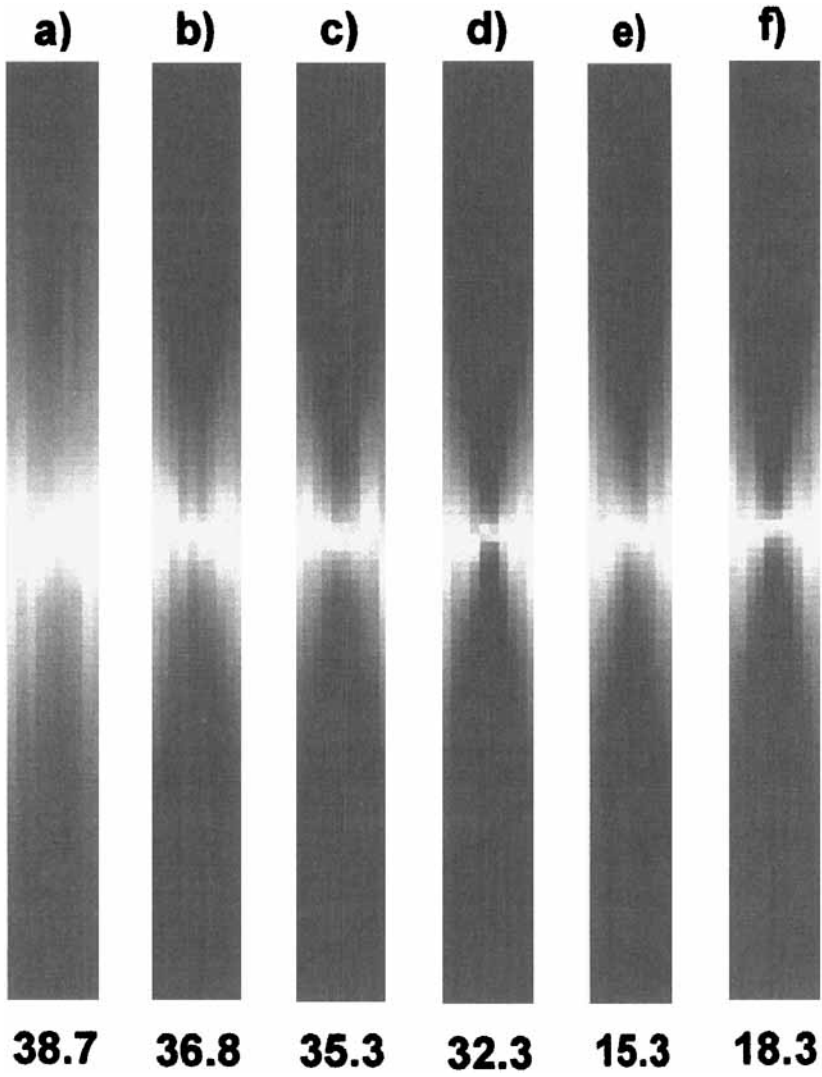

FIGURE 7 Stochastic simulations of the 2D polarity distribution: a) NPP, 120 × 15 μm^2(crystal size) with summation over an area of ~ 1 μm^2 (spot size). The macroscopic area of 120 × 15 μm^2 corresponds to 6 SPEM spots of 20 × 20 μm^2. b)-d) Same type of information, but for a decreasing $E_{AA} - E_{AD}$ difference (as in Fig. 5). e)-f) Similar to b)-d), but shown as a function of an increasing $E_{AA} - E_{DD}$ difference. The colour intensity is a measure of the *local net polarity*. Colour code: red = ↑, blue = ↓, white = zero (corresponding to the SPEM colours, see Fig. 1). Changing the relevant energy difference is leading to a more pronounced cone geometry (energies in kJ mol^{-1}) (See Color Plate XX at the back of this issue)

As a result of a previous analysis based on X-ray data[12] we concluded that $E_{AA} - E_{DD} > 6$ kJ mol^{-1}and $E_{AA} - E_{AD} > 14$ kJ mol^{-1}. Following these results, most probable lengths figure out to be much shorter. In summary, we can say that both the SPEM and the X-ray analysis do not permit us to derive more precise data on L_A and L_D of PHTP-NPP. An experimental resolution of at least ~ 1 μm would be necessary. This might be provided by new techniques, in particular near-field optical second-harmonic microscopy (SHG-SNOM)[3] and electrostatic force microscopy[4]. While this manuscript was reviewed, we improved the lateral resolution of the SPEM surface mode to 2.5 μm by lowering the current noise level to 1 fA[13].

5. CONCLUSIONS

Layer by layer scanning pyroelectric microscopy can provide a *tomographic* tool for the investigation of molecular crystals featuring a spatially inhomogeneous polarisation. In cases where thinning of samples is feasible within less than 10 μm per step, a lateral and depth resolution of the same order can be achieved. Up to now, SPEM is the only experimental technique which can reveal the bi-polar structure of PHTP inclusion compounds. However, most recent developments in the field of *scanning near field optical microscopy* might represent alternative tools, providing a lateral resolution down to probably 10–100 nm[3]. Experiments along these lines are in progress. Following Eqs. (2) – (4), the polarity evolution is essentially driven by $|E_{AA} - E_{DD}|$, whereas phenomena of typical chain length formation (L_A, L_D) are due to $|E_{AA} - E_{AD}|$ for $E_{AA} > E_{DD}$, and $|E_{DD} - E_{AD}|$ for $E_{DD} > E_{AA}$. In summary, we have developed the mathematical tools for simulating the real structure of *macroscopic* crystals, although the present computing facilities allow us only to present maps featuring a lateral resolution of ~ 1 μm if compared to the experimental resolution of SPEM which was 20 μm in the case of PHTP inclusion compounds.

Acknowledgements

This work was supported by the Swiss National Science Foundation [NFP 36 (4036–0439932) and NF (21–50828.97)]. We thank H. Quintel for giving advice to program the stochastic simulations, and Dr. O. König (Molecular Simulations Ltd., Cambridge, U.K.) for the calculation of the intermolecular interaction energies.

References

[1] J. Hulliger, *Z. Kristallogr.*, **213**, 441 (1998), J. Hulliger, *Z. Kristallogr.*, **214**, 9 (1999).

[2] J. Hulliger and P. J. Langley, *Chem. Comm.*, 2557 (1998).
[3] S. I. Bozhevolnyi, B. Vohnsen and K. Pedersen, *Opt. Comm.*, **150**, 49 (1998); I. I. Smolyaninov, A. V. Zayats and Ch. C. Davis, *Opt. Lett.*, **22**, 1592 (1997).
[4] E. Soergel, W. Krieger and V. I. Vlad, *Appl. Phys. A*, **66**, 337 (1998).
[5] M. Flörsheimer, M. Bösch, C. Brillet, M. Wierschem and H. Fuchs, *Adv. Mater.*, **9**, 1061 (1997); J. Vydra and M. Eich, *Appl. Phys. Lett.*, **72**, 275 (1998).
[6] A. Quintel, J. Hulliger and M. Wübbenhorst, *J. Phys. Chem. B*, **102**, 4277 (1998).
[7] G. J. Klap, S. M. van Klooster, M. Wübbenhorst, J. C. Jansen, H. van Bekkum and J. van Turnhout, *J. Phys. Chem. B*, **102**, 9518 (1998).
[8] J. Hulliger, O. König and R. Hoss, *Adv. Mater.*, **7**, 719 (1995); R. Hoss, O. König, V. Kramer-Hoss, U. Berger, P. Rogin and J. Hulliger, *Angew. Chem. Ed. Int. Engl.*, **35**, 1664 (1996).
[9] M. Wübbenhorst, J. van Turnhout, A. Quintel, J. Hulliger, *J. Appl. Phys.*, to be submitted (1999).
[10] J. Hulliger, A. Quintel, M. Wübbenhorst, P. J. Langley, S. W. Roth and P. Rechsteiner, *Opt. Mater.*, **9**, 259 (1998); J. Hulliger, P. J. Langley, O. König, S. W. Roth, A. Quintel and P. Rechsteiner, *Pure Appl. Opt.*, **7**, 221 (1998); S. W. Roth, P. J. Langley, A. Quintel, M. Wübbenhorst, P. Rechsteiner, P. Rogin, O. König and J. Hulliger, *Adv. Mater.*, **10**, 1543 (1998).
[11] Collinear intermolecular interaction energies were calculated by applying the DREIDING 2.20.1 force field. Atomic charges for the calculation of the Coulombic interactions were obtained from MOPAC, using the MNDO approximation. Both sets of calculations were performed using CERIUS 2 software (Molecular Simulations Ltd.).
[12] O. König, H.-B. Bürgi, T. Armbruster, J. Hulliger and T. Weber, *J. Am. Chem. Soc.*, **119**, 10632 (1997).
[13] G. J. Klap, M. Wübbenhorst, H. van Koningsveld, H. van Bekkum and J. van Turnhout, *Chem. Mater.*, 1999, in press.